Helmholtz-Zentrum Geesthacht
Zentrum für Material- und Küstenforschung

Final Draft
of the original manuscript:

Zhao, D.; Ebel, T.; Yan, M.; Qian, M.:

Trace Carbon in Biomedical Beta-Titanium Alloys: Recent Progress

In: JOM: Journal of the Minerals, Metals and Materials Society (2015)
Springer

DOI: 10.1007/s11837-015-1590-6

Trace carbon in biomedical beta−titanium alloys: Recent progress

D. Zhao [a], T. Ebel [b], M. Yan [c]*, M. Qian [d]*

Affiliation:

[a] College of Biology, Hunan University, 410082 Changsha, P. R. China

[b] Helmholtz-Zentrum Geesthacht, Institute of Materials Research, Max-Planck-Str. 1, 21502 Geesthacht, Germany

[c] Department of Materials Science and Engineering, South University of Science and Technology of China, 518055 Shenzhen, P. R. China

[d] RMIT University, School of Aerospace, Mechanical and Manufacturing Engineering, Centre for Additive Manufacturing, Melbourne, VIC 3001, Australia

*Corresponding author:

Dr. Ming Yan, Tel.: +86-755-88018967, E-mail address: yanm@sustc.edu.cn;

Prof. Ma Qian, Tel: +61-3-99254491, E-mail address: ma.qian@rmit.edu.au

Abstract:

Owing to their relatively low Young's modulus, high strength, good resistance to corrosion and excellent biocompatibility, β-titanium (Ti) alloys have shown great potential for biomedical applications. In β-Ti alloys, carbon can exist in the form of titanium carbide (TiC_x) as well as interstitial atoms. The Ti-C binary phase diagram predicts a minimum carbon solubility value of 0.08 wt.% in β-Ti, which has been used as the carbon limit for a variety of β-Ti alloys. However, noticeable grain boundary TiC_x particles have been observed in β-Ti alloys at impurity levels of carbon well

below the predicted 0.08 wt.%. This review focuses its attention on the trace carbon (≤ 0.08 wt.%) in biomedical β-Ti alloys containing niobium (Nb) and molybdenum (Mo), and discusses the nature and precipitation mechanism of the TiC_x particles in these alloys.

Key words: Biomedical β-Ti alloys; Carbon; Titanium carbide; Carbon solubility

1. Introduction

New generation aluminum (Al)- and vanadium (V)-free, biomedical β-Ti alloys are being widely pursued for at least two good reasons [1]: (a) the Al and V elements in the Ti-6Al-4V alloy are found to be associated with some long-term health problems, most notably Alzheimer disease, neuropathy and osteomalacia due to the release of both elements to human body [2]; and (b) they offer lower Young's modulus than Ti (~100 GPa) and Ti-6Al-4V (~110GPa); in particular some β-Ti alloys can have Young's modulus close to human bones' (~30GPa) [3]. This helps to mitigate the so-called "stress-shield" impact arising from the mismatch in modulus between the implant material and human bone. When further compared to CP-Ti, β-Ti alloys generally show higher strength and hardness, making them more suitable for applications such as bone screws, plates and similar products [1]. As a result, a variety of biomedical β-Ti alloys, for instances, Ti-35Nb-5Ta-7Zr-0.4O [4] and Ti-15Mo [5], have been developed over the last two decades. It is noted that many such biomedical

β-Ti alloys contain a significant level of Nb and/or Mo (β-stabilizers), assisted with a combination of Zr and Sn, which are neutral elements to Ti.

Impurity elements (e.g. O, N, H and Fe) can noticeably affect the microstructure and/or mechanical properties of Ti and Ti alloys. For example, a small increase in oxygen content (from 0.25 wt.% to 0.33 wt.%) can reduce the ductility of Ti-6Al-4V from 15 % to 8 % [6] (which occurs similarly to a β-Ti alloy (Ti-29Nb-13Ta-4.6Zr) [7]), while the presence of 0.3 wt.% Fe can significantly refine the β-Ti grains in Grade 7 Ti [8]. However, compared with O, Fe, N and H, the role of trace carbon (C) in β-Ti alloys has not received adequate attention, especially in biomedical β-Ti alloys. Table 1 lists the carbon limits for several important near β- and β-Ti alloys, two commercial biomedical β-Ti alloys, the Grade 1 commercially pure Ti (CP-Ti) and Ti-6Al-4V. The carbon limits are set as either (0.08-0.10) wt.% or 0.05 wt.%. In fact, this is also the case for most other Ti materials including other β-Ti alloys. The underlying reason can be inferred from Fig. 1, which shows the Ti-C binary phase diagram up to 1.2 wt.% of C, predicted using Thermo-Calc Software 2008 and Ti alloys database V3 (TTTI3). The formation of titanium carbide, however, will generally lead to the following consequences [9-11]: (a) raising chemical inhomogeneity and therefore results in a reduced corrosion resistance; (b) forming brittle ceramic phases in the microstructure and therefore leads to a reduced elongation as well as fatigue property; and (c) enlarging the overall Young's modulus due to the high modulus of titanium carbide itself and therefore widens the mismatch

between the implant Ti material and human bones in terms of modulus. These negative impacts on mechanical performance and corrosion resistance can be evidenced from a variety of studies such as [12, 13] as well as the results to be disclosed below for the as-sintered Ti-Nb alloys (please see Table 3 and relevant contents). In the biological aspect, continuous titanium carbide coating may improve biocompatibility and osseointegration compared to uncoated Ti but this should not be applicable to the discontinuous, impurity-induced titanium carbide particles observed by the several independent studies [14, 15].

To avoid the formation of titanium carbide (TiC_x), the carbon content in pure titanium should be limited to less than 0.08 wt.% by Fig. 1. This prediction has served as the theoretical basis for defining the carbon limit in most Ti alloys including many near β- and β-Ti materials while a reduced carbon limit, specified as 0.05 wt.%, has been used for some near β- and β-Ti alloys (with the exception of Ti-15V-3Cr-3Al-3Sn as a sheet alloy, whose carbon limit is set as 0.03 wt.% [16]). For biomedical β-Ti alloys such as Ti-13Nb-13Zr and Ti-15Mo listed in Table 1, the carbon limit has simply followed the predicted value of (0.08-0.10) wt.% for pure Ti. In summary, the role of trace C in biomedical β-Ti alloys has not received adequate attention as yet compared with other common impurities (O, Fe, N and H). It should be noted that Fig. 1 points out at room temperature the stable phase is α-Ti or a combination of α-Ti and TiC phases. Beta-Ti phase, however, can be retained to room temperature as either stable or metastable

phase as long as there are sufficient β stablisers such as the Nb and Mo elements as mentioned already.

Recent studies on a few biomedical β-Ti alloys have shown that TiC_x particles can form in these alloys at carbon contents well below their respective limits set by the ASTM Standard Specifications [10, 11, 17]. This paper reviews the recent progress in understanding the role of trace C in biomedical β-Ti alloys based on several detailed studies of trace C in Ti-Nb and Ti-Mo alloys. The precipitation mechanism of the TiC_x particles in these alloys is discussed according to the influence of Nb and Mo on the phase diagram and the change in the lattice parameter of the resulting β-Ti phase. The selection of the Ti-Nb and Ti-Mo systems is because Nb and Mo are two important alloying elements for biomedical β-Ti alloys. For instance, successful biomedical β-Ti alloys that have already been developed based on alloying with Nb and/or Mo include Ti-13Nb-13Zr [18], Ti-35Nb-5Ta-7Zr [19], Ti-29Nb-13Ta-4.6Zr [20], Ti-24Nb-4Zr-8Sn [21], Ti-15Mo [22], and Ti-25Nb-2Mo-4Sn [23]. In fact, many of the aforementioned β-type Ti-Nb and Ti-Mo alloys are believed to be the second-generation biomaterials to replace partially or even fully the first-generation Ti biomaterials (e.g. CP-Ti and Ti-6Al-4V) that were developed in the years of 1950-1990 [1].

2. Carbon in Ti-Nb alloys

Owing to their low elastic modulus and superior biocompatibility, Ti-Nb based alloys

are attracting increasing attention for biomedical applications [24]. Several studies have dealt with the role of carbon in these alloys. Recently, Hosoda et al. [25] have shown that an addition of (0.2-0.5) wt.% of carbon to a Ti-27at.%Nb, i.e., Ti-41wt.%Nb, alloy can refine the grain structure (the grain size decreased with increasing carbon concentration), due to the grain boundary pinning effect of TiC_x particles. In addition, the critical stress for slip also increased as a result of the formation of carbide. However, the addition of such a level of carbon as an alloying element often risks embrittling the alloy due also to the formation of carbides. One exception is that reported by Li et al. [26], who introduced more than 0.1 wt.% of C to a β-Ti alloy of Ti-25V-15Cr-2Al (wt.%) and achieved a dramatic increase in tensile elongation (from less than 2 % to more than 20 %). The reason was attributed to the formation of Ti_2C particles, which gettered oxygen from the Ti matrix leading to much improved tensile ductility. However, the formation of Ti_2C carbides in other β-Ti alloys resulted in a substantial decrease in tensile elongation as will be shown below. Hence, it is uncommon to introduce extra carbon to β-Ti alloys. Rather the carbon content should be strictly controlled in most cases.

A more recent study by Zhao et al. [11] has looked at the influence of carbon as a normal impurity on the microstructure and mechanical properties of three Ti-Nb binary alloys (Ti-10Nb, Ti-16Nb and Ti-22Nb, all in wt.%), processed by metal injection moulding (MIM) and sintering. Gas-atomized Ti powder (< 45 μm) and hydride/dehydride Nb powder (< 110 μm) were used to fabricate the samples.

Additionally, CP-Ti samples were fabricated by the same MIM process as a point of reference. After chemical and thermal debinding, all samples were sintered at 1500 ℃ for 4 h. Table 2 lists the impurity levels of the starting powders and the as-sintered samples. Due to reactions with the residual polymeric binder during thermal debinding and sintering, the carbon content of the as-sintered samples increased by about (0.045-0.050) wt.% compared to the carbon content of the starting powders but the total C content is still clearly below 0.08 wt.%. Acicular TiC_x particles were observed in all the as-sintered Ti-Nb samples, while, the as-sintered CP-Ti samples were free of the formation of carbides. Fig. 2 shows the microstructures of the as-sintered CP-Ti and Ti-22Nb samples. The strip-shaped TiC_x particles were found residing on the grain boundaries.

A detailed microstructure study of the as-sintered Ti-22Nb alloy was performed using transmission electron microscopy (TEM) as shown in Fig. 3, in order to better understand the nature of the TiC_x particles. The selected area electron diffraction (SAED) pattern of the TiC_x particle revealed that the carbide phase exhibited a face-centered-cubic (FCC) structure with lattice parameter $\boldsymbol{a}$ = 4.3 Å. The extra diffraction maxima at various zone axes with much lower intensity suggest that the TiC_x particle should be *Fd3m*-Ti_2C, consistent with the titanium carbide (Ti_2C) identified in the Ti-25V-15Cr-2Al (wt.%) alloy [26]. However, it should be pointed out that the conditions under which Ti_2C, rather than TiC, forms in a β-Ti alloy remains to be unanswered question. The following crystallographic relationship was

identified between the particle and its surrounding body-centered-cubic (BCC) β-Ti matrix: $\left(11\bar{1}\right)_{Ti_2C}//\left(110\right)_{\beta-Ti}$ and $\left[011\right]_{Ti_2C}//\left[001\right]_{\beta-Ti}$. Besides, reflections from hexagonal-close-packed (HCP) α-Ti were also observed in Fig. 3d. According to Sekimoto et al. [27], a small amount of *Fd3m*-Ti_2C particles may have transformed into α-Ti in the β-Ti matrix. For example, the (111) plane of the *Fd3m*-Ti_2C could transform itself in to the (0001) plane of α-Ti through sliding, with the stacking sequences changing from the ABCABC type in the former lattice to the ABAB type in the latter. In this case, the crystallographic relationship between α-Ti and *Fd3m*-Ti_2C will follow: $\left(111\right)_{Ti_2C}//\left(0001\right)_{\alpha-Ti}$.

In order to eradicate the influence of residual porosity on the mechanical properties, the as-sintered CP-Ti and Ti-Nb alloys were subjected to hot isostatic pressing (HIP). Table 3 lists the area fractions of carbides and tensile properties of the as-HIPed CP-Ti and Ti-Nb samples. The amount of TiC_x particles showed a clear dependency on the Nb content. As a result, the tensile elongation of the as-HIPed, pore-free Ti-Nb alloys decreased linearly with increasing Nb content (see Table 3). However, the tensile strength showed the opposite trend, which can be attributed to the strengthening effect spawned by the carbide particles.

Fig. 4 shows a longitudinal section of the fractured tensile specimen of the as-HIPed Ti-22Nb alloy including part of the fracture surface profile. Microcracks were found to have initiated from the carbide particles. In addition, most carbide particles were

fragmented showing cross-section microcracks perpendicular to the tensile direction. These observations explain the linear drop in tensile elongation with increasing Nb content, which corresponds to the nearly linear increase in the area fraction of carbides.

In addition to the MIM-processed Ti-Nb binary alloys, carbide particles were also observed in an MIM-processed and HIPed Ti-24Nb-4Sn-8Zr (Ti-2448) alloy containing a super-low level of carbon (0.009 wt.%) [28]. Similar to the as-HIPed Ti-Nb alloys discussed above, this as-HIPed Ti-2448 alloy showed very low tensile elongation (about 1.8 %), due to the formation of carbides with an area fraction of around 1.5 %.

3. Carbon in Ti-Mo alloys

Mo is the most effective β stabilizer: an introduction of 8 wt.% of Mo is sufficient to retain the β-Ti phase quenched from the β field [29], whereas, it requires 22 wt.% of Nb or 52 wt.% of Ta to stabilize the β-phase. The ASTM standard F 2066-2008 defined the maximum carbon limit for wrought Ti-15Mo as 0.10 wt.% for surgical implant applications. However, TiC_x particles were observed in Ti-15Mo alloy samples containing just 0.032 wt.% of C [10]. The Ti-15Mo alloy was fabricated by uniaxial cold compaction of the mixture of titanium hydride (TiH_2) powder (99.5 % purity, 95-106 μm) and elemental Mo powder (99.5 % purity, <63 μm), followed by sintering at 1350 ℃ for 2 h. Fig. 5a shows an SEM image of the primary α-Ti

(designated as α_p-Ti), β-Ti matrix and carbide particles in the as-sintered Ti-15Mo alloy. The grain boundary TiC_x particles exhibited a similar strip-like shape as observed in the MIM-processed Ti-Nb alloys. Fig. 5b presents the SAED patterns of the TiC_x particles and the adjacent β-Ti matrix. The TiC_x particles in the as-sintered Ti-15Mo alloy exhibited the structure of *Fd3m*-Ti_2C with lattice parameter ***a*** = 4.29 Å, which is similar to the Ti_2C formed in the MIM-processed Ti-Nb alloys and those reported in Ti-25V-15Cr-2Al (wt.%) alloy [26]. Semi-coherent orientation relationships were identified between the carbide particles and the β-Ti matrix, and one of them is $\left(11\bar{1}\right)_{Ti_2C}//\left(110\right)_{\beta-Ti}$ and $\left[112\right]_{Ti_2C}//\left[113\right]_{\beta-Ti}$.

4. Titanium carbide precipitation mechanism in β-Ti

As shown above, acicular TiC_x particles were observed in β-Ti alloys with carbon contents clearly below the critical carbon limit predicted for pure Ti (0.08 wt.%). Also, it has been found that the amount of carbides increased with increasing concentration of the β-stabilizers (Table 3). It is thus necessary to assess the carbon solubility in Ti alloys with β-stabilizers.

Fig. 6 shows the Thermo-Calc predictions of the pseudo-binary (Ti-Nb)-C phase diagrams with the Nb contents of 10 wt.%, 16 wt.% and 22 wt.%. There is a notable decrease in carbon solubility with increasing Nb content. The minimum carbon contents in the β-(Ti-Nb) phase in the Ti-10Nb, Ti-16Nb and Ti-22Nb alloys are 0.051 wt.% at 812 ℃, 0.036 wt.% at 718 ℃, and 0.021 wt.% at 735 ℃, respectively.

The precipitation mechanism of TiC_x particles can be understood using the pseudo-binary (Ti-Nb)-C phase diagrams. At the sintering temperature of 1500 ℃, the carbon solubility levels in Ti-10Nb, Ti-16Nb and Ti-22Nb alloys are 0.307 wt.%, 0.278 wt.% and 0.251 wt.%, respectively, compared to the total carbon content of (0.05-0.07) wt.% in each alloy (see Table 2). Consequently, all the carbon should be in solid solution at the end of isothermal sintering at 1500 ℃ for 4 h. During subsequent cooling, the solubility of carbon in β-Ti phase decreases with decreasing temperature, reaching a minimum of 0.051 wt.% at 812 ℃ for Ti-10Nb, a minimum of 0.036 wt.% at 718 ℃ for Ti-16Nb and a minimum of 0.021 wt.% at 735 ℃ for Ti-22Nb. Precipitation of carbides is thus expected in this stage. As temperature further decreases, although the solubility of carbon increases to 0.161 wt.% at 723 ℃ for Ti-10Nb, 0.117 wt.% at 678 ℃ for Ti-16Nb and 0.089 wt.% at 641 ℃ for Ti-22Nb (see Fig. 6), because of the relatively low temperature, no dissolution of carbides is expected. The precipitation of carbides thus mainly occurs during cooling before reaching the minimum-carbon-solubility temperature. Further precipitation during slow cooling below 500 ℃ (see Fig. 2) is also possible.

Similar to the pseudo-binary (Ti-Nb)-C phase diagrams shown in Fig. 6, the pseudo-binary (Ti-15Mo)-C phase diagram constructed using Thermo-Calc, shown in Fig. 7, also revealed a significant decrease of carbon solubility in β-Ti due to the introduction of the 15 wt.% of Mo. This minimum carbon solubility in the β-Ti phase

of the Ti-15Mo alloy is 0.006 wt.% at 735 ℃ compared to 0.08 wt.% of C without Mo (see Fig. 1). This critical carbon level (0.006 wt. %) is far below the actual carbon content of the MIM-processed Ti-15Mo alloy, which is about 0.05-0.07 wt.% [10]. As a consequence, there was noticeable formation of carbides in the Ti-15Mo alloy despite the presence of just a trace level of carbon (0.05-0.07) wt. %.

The above observations also occur to Ti-V based β-Ti alloys, although V is not preferred for biomedical applications [30]. Fig. 8 shows the pseudo-binary (TI-15V)-C phase diagram up to 0.5 wt.% of C predicted using Thermo-Calc software. The minimum solubility of C in β-(Ti-V) decreased from 0.08 wt.% without V (see Fig. 1) to just 0.0113 wt.% (see Fig. 8). Consequently, grain boundary carbides are readily observable in an aged MIM-processed Ti-15V-3Al-3Sn-3Cr (Ti-15333) alloy which contained only 0.046 wt.% of C (see Fig. 9).

The significant impact of the β-stabilizers particularly Nb and Mo (also including V) on the carbon solubility in the β-Ti matrix can be understood according to the change of the lattice parameter of β-Ti after adding these alloying elements. For instance, Severino Martins et al. [31] have found that the addition of Mo reduces the lattice parameter of the β-phase in pure Ti. At room temperature, the lattice parameter of pure β-Ti is 3.31 Å (JCPDS PDF database # 44-1288), while, that of β-(Ti-15Mo) is 3.26 Å [31]. Similarly, the lattice parameter of β-(Ti-22Nb) was determined to be 3.277 Å by high energy X-ray diffraction measurements [32]. In the β-Ti lattice, the

addition of β-stabilizers such as Mo and Nb reduces the tetrahedral vacancy space, and therefore leads to a significant decrease of the carbon solubility, favoring the formation of TiC_x particles.

5. Summary and future work

This work aims at the understanding of the influence of trace carbon (≤ 0.08 wt.%) on microstructure and mechanical properties of β-Ti alloys. Acicular TiC_x precipitates have been observed in a variety of β-Ti alloys, such as Ti-Nb and Ti-Mo alloys. These carbides are usually distributed along grain boundaries. The TiC_x particles exhibit an FCC structure with lattice parameter of about $\boldsymbol{a}$ = 4.3 Å, and have been determined to be *Fd3m*-Ti_2C. The carbide particles and the adjacent matrix show a crystallographic relationship which can be described as: $(111)_{Ti_2C}//(0001)_{\alpha-Ti}//(110)_{\beta-Ti}$. These grain-boundary Ti_2C particles have proved to be highly detrimental to the tensile ductility of these alloys and are expected to be also detrimental to the fatigue property and corrosion resistance of the alloy due to the microstructural homogeneity.

The precipitation of the Ti_2C carbides results from the significantly reduced carbon solubility in the β-Ti matrix after introducing the β-stabilizing elements. The addition of these elements decreases the lattice parameter of the BCC β-Ti matrix, leading to less tetrahedral vacancy space. Thus less carbon can stay in the matrix as interstitial atoms, which therefore leads to the precipitation of carbides.

Owing to their negative impacts on microstructural homogeneity and mechanical property, it is necessary to avoid the formation of the TiC_x precipitates in the biomedical β-Ti alloys. However, this implies that the carbon content in biomedical β-Ti alloys should be controlled to be less than 0.006 wt.%. This may prove to be impractical or too costly to do so. A remedy is to apply a proper heat treatment process, followed by quenching. This needs to be explored in the future for these alloys. In addition, it would be useful to understand why Ti_2C rather than TiC forms in all these β-Ti alloys.

Acknowledgements

This research was funded by Young Teacher Growth Plan (File No. 531107040850). M. Qian acknowledges the financial support of the Australian Research Council (ARC) through ARC LP130100913. D. Zhao and T. Ebel are grateful to Prof. Florian Pyczak and Prof. Regine Willumeit from Helmholtz-Zentrum Geesthacht for the assistance and input. Dr. Shenglu Lu of The University of Queensland is acknowledged for the calculations of the pseudo-binary (Ti-15V)-C phase diagram.

References

[1] M. Geetha, A. K. Singh, R. Asokamani, A. K. Gogia, Ti based biomaterials, the ultimate choice for orthopaedic implants - A review, Progress in Materials Science, 54 (2009) 397-425.

[2] M. Niinomi, M. Nakai, J. Hieda, Development of new metallic alloys for biomedical applications, Acta Biomaterialia, 8 (2012) 3888-3903.

[3] L.C. Zhang, D. Klemm, J. Eckert, Y.L. Hao, T.B. Sercombe, Manufacture by selective laser melting and mechanical behavior of a biomedical Ti–24Nb–4Zr–8Sn alloy, Scripta Materialia, 65 (2011) 21-24.

[4] T. Saito, T. Furuta, J.-H. Hwang, S. Kuramoto, K. Nishino, N. Suzuki, R. Chen, A. Yamada, K. Ito, Y. Seno, Multifunctional Alloys Obtained via a Dislocation-Free Plastic Deformation Mechanism, Science, 300 (2003) 464-467.

[5] W.F. Ho, C.P. Ju, J.H. Chern Lin, Structure and properties of cast binary Ti–Mo alloys, Biomaterials, 20 (1999) 2115-2122.

[6] M. Yan, M.S. Dargusch, T. Ebel, M. Qian, A transmission electron microscopy and three-dimensional atom probe study of the oxygen-induced fine microstructural features in as-sintered Ti–6Al–4V and their impacts on ductility, Acta Materialia, 68 (2014) 196-206.

[7] M. Nakai, M. Niinomi, T. Akahori, H. Tsutsumi, M. Ogawa, Effect of Oxygen Content on Microstructure and Mechanical Properties of Biomedical Ti-29Nb-13Ta-4.6Zr Alloy under Solutionized and Aged Conditions, Materials Transactions, 50 (2009) 2716-2720.

[8] M. Yan, M. Qian, T.T. Song, M.S. Dargusch, X.S. Wei, Significant α-phase growth confinement in Grade 4 titanium and substantial β-phase refinement in Grade 7 titanium, MRS Communications, 4 (2014) 183-188.

[9] H. Choe, S. Abkowitz, S.M. Abkowitz, D.C. Dunand, Mechanical properties of Ti–W alloys reinforced with TiC particles, Materials Science and Engineering: A, 485 (2008) 703-710.

[10] M. Yan, M. Qian, C. Kong, M.S. Dargusch, Impacts of trace carbon on the microstructure of as-sintered biomedical Ti-15Mo alloy and reassessment of the maximum carbon limit, Acta Biomaterialia, (2014) In press.

[11] D. Zhao, K. Chang, T. Ebel, M. Qian, R. Willumeit, M. Yan, F. Pyczak, Microstructure and mechanical behavior of metal injection molded Ti-Nb binary alloys as biomedical material, Journal of the Mechanical Behavior of Biomedical Materials, 28 (2013) 171-182.

[12] R. Banoth, R. Sarkar, A. Bhattacharjee, T.K. Nandy, G.V.S. Nageswara Rao, Effect of boron and carbon addition on microstructure and mechanical properties of metastable beta titanium alloys, Materials & Design, 67 (2015) 50-63.

[13] A. Shanaghi, P.K. Chu, A.R. Sabour Rouhaghdam, R. Xu, T. Hu, Structure and corrosion resistance of Ti/TiC coatings fabricated by plasma immersion ion implantation and deposition on nickel–titanium, Surface and Coatings Technology, 229 (2013) 151-155.

[14] M. Brama, N. Rhodes, J. Hunt, A. Ricci, R. Teghil, S. Migliaccio, C.D. Rocca, S. Leccisotti, A. Lioi, M. Scandurra, G. De Maria, D. Ferro, F. Pu, G. Panzini, L. Politi, R. Scandurra, Effect of titanium carbide coating on the osseointegration response in vitro and in vivo, Biomaterials, 28 (2007) 595-608.

[15] G. Longo, M. Girasole, G. Pompeo, A. Cricenti, C. Misiano, A. Acclavio, A.C. Tizzoni, L. Mazzola, P. Santini, L. Politi, R. Scandurra, Effect of titanium carbide coating by ion plating plasma-assisted deposition on osteoblast response: A chemical, morphological and gene expression investigation, Surface and Coatings Technology, 204 (2010) 2605-2612.

[16] J. Matthew J. Donachie, Titanium: a technical guide., ASM INTERNATIONAL, Materials Park,

Ohio, 2000.
[17] D. Zhao, K. Chang, T. Ebel, M. Qian, R. Willumeit, M. Yan, F. Pyczak, Titanium carbide precipitation in Ti-22Nb alloy fabricated by metal injection moulding, Powder Metallurgy, 57 (2014) 2-4.
[18] K.S. Suresh, N.P. Gurao, S. Singh D, S. Suwas, K. Chattopadhyay, S.V. Zherebtsov, G.A. Salishchev, Effect of equal channel angular pressing on grain refinement and texture evolution in a biomedical alloy Ti13Nb13Zr, Materials Characterization, 82 (2013) 73-85.
[19] C.R.M. Afonso, P.L. Ferrandini, A.J. Ramirez, R. Caram, High resolution transmission electron microscopy study of the hardening mechanism through phase separation in a β-Ti–35Nb–7Zr–5Ta alloy for implant applications, Acta Biomaterialia, 6 (2010) 1625-1629.
[20] M. Niinomi, Fatigue performance and cyto-toxicity of low rigidity titanium alloy, Ti–29Nb–13Ta–4.6Zr, Biomaterials, 24 (2003) 2673-2683.
[21] Y. Yang, P. Castany, M. Cornen, F. Prima, S.J. Li, Y.L. Hao, T. Gloriant, Characterization of the martensitic transformation in the superelastic Ti–24Nb–4Zr–8Sn alloy by in situ synchrotron X-ray diffraction and dynamic mechanical analysis, Acta Materialia, 88 (2015) 25-33.
[22] A. Kazek-Kęsik, M. Krok-Borkowicz, E. Pamuła, W. Simka, Electrochemical and biological characterization of coatings formed on Ti–15Mo alloy by plasma electrolytic oxidation, Materials Science and Engineering: C, 43 (2014) 172-181.
[23] S. Guo, Q. Meng, G. Liao, L. Hu, X. Zhao, Microstructural evolution and mechanical behavior of metastable β-type Ti–25Nb–2Mo–4Sn alloy with high strength and low modulusMicrostructural evolution and mechanical behavior of metastable β-type Ti–25Nb–2Mo–4Sn alloy with high strength and low modulusretain--&gt, Progress in Natural Science: Materials International, 23 (2013) 174-182.
[24] A. Terayama, N. Fuyama, Y. Yamashita, I. Ishizaki, H. Kyogoku, Fabrication of Ti–Nb alloys by powder metallurgy process and their shape memory characteristics, Journal of Alloys and Compounds, 577, Supplement 1 (2013) S408-S412.
[25] H. Hosoda, Y. Horiuchi, T. Inamura, K. Wakashima, H.Y. Kim, S. Miyazaki, Effect of Carbon Addition of Shape Memory Properties of TiNb Alloys, Materials Science Forum, 638-642 (2010) 2046-2051.
[26] Y.G. Li, P.A. Blenkinsop, M.H. Loretto, D. Rugg, W. Voice, Effect of carbon and oxygen on microstructure and mechanical properties of Ti-25V-15Cr-2Al (wt.%) alloys, Acta Materialia, 47 (1999) 2889-2905.
[27] W. Sekimoto, H. Tsuda, S. Mori, Effects of Chromium and Nitrogen Contents on Microstructural Changes in TiC Particles in (alpha plus beta)- and beta-Titanium Matrix Composites, Materials Transactions, 53 (2012) 1405-1411.
[28] F. Kafkas, T. Ebel, Metallurgical and mechanical properties of Ti–24Nb–4Zr–8Sn alloy fabricated by metal injection molding, Journal of Alloys and Compounds, 617 (2014) 359-366.
[29] N.T.C. Oliveira, G. Aleixo, R. Caram, A.C. Guastaldi, Development of Ti–Mo alloys for biomedical applications: Microstructure and electrochemical characterization, Materials Science and Engineering: A, 452–453 (2007) 727-731.
[30] H.M. Silva, S.G. Schneider, C.M. Neto, Study of nontoxic aluminum and vanadium-free titanium alloys for biomedical applications, Materials Science and Engineering: C, 24 (2004) 679-682.
[31] J.R. Severino Martins, C.R. Grandini, Structural characterization of Ti-15Mo alloy used as biomaterial by Rietveld method, Journal of Applied Physics, 111 (2012) 083535-083535-083538.
[32] D. Zhao, Metal Injection Moulding of Titanium-Niobium Alloys for Biomedical Applications., in:

Fakultät Maschinenbau, Elektrotechnik und Wirtschaftsingenieurwesen, Brandenburgische Technische Universität Cottbus-Senftenberg, Cottbus, 2014.
[33] M. Semlitsch, Titanium alloys for hip joint replacements, Clinical Materials, 2 (1987) 1-13.

Figure captions

Fig. 1. Ti-C phase diagram up to 1.2 wt.% of carbon, predicted using Thermo-Calc Software 2008 and Ti alloys database V3 (TTTI3) (Courtesy of Yan et al. [10]).

Fig. 2. Microstructures of MIM-processed and sintered (a) CP-Ti and (b) Ti-22Nb samples (scanning electron microscopy (SEM) images). The inset in Fig. 2b shows the EDS results of carbide particles.

Fig. 3. TEM micrograph and SAED patterns of the as-sintered Ti-22Nb alloy (a) the bright field image, (b) a SAED pattern showing Ti_2C reflections from [011]; (c) a SAED pattern showing reflections of the matrix around the Ti_2C precipitate, the pattern was found to be β-Ti reflections from [001] and (d) a SAED pattern showing both Ti_2C and β-Ti reflections as well as several diffraction spots from α-Ti (Courtesy of Zhao et al. [11]).

Fig. 4. SEM micrograph along the longitudinal section of a fractured as-HIPed Ti-22Nb sample showing fragmented carbide particles and microcracks.

Fig. 5. (a) SEM image of the as-sintered Ti-15Mo alloy and (b) an overlap of the SAED patterns of the TiC_x particles and the adjacent β-Ti matrix (Courtesy of Yan et al. [10]).

Fig. 6. Pseudo-binary phase diagrams of (Ti-10Nb)-C, (Ti-16Nb)-C and (Ti-22Nb)-C up to 0.5 wt.% of carbon predicted using Thermo-Calc software (Courtesy of Zhao et al. [32]).

Fig. 7. Pseudo binary (Ti-15Mo)-C phase diagram up to 1.0 wt.% of C predicted using

Thermo-Calc software (Courtesy of Yan et al. [10]).

Fig. 8. Pseudo binary (Ti-15V)-C phase diagram up to 0.5 wt.% of carbon predicted using Thermo-Calc software.

Fig. 9. Microstructure of aged MIM-processed Ti-15V-3Al-3Sn-3Cr (Ti-15333) alloy. Samples were sintered at 1400 ℃ for 2 h after MIM and then aged at 500 ℃ for 12 h. The C, O and N contents were about 0.046 wt.%, 0.21 wt.% and 0.024 wt.%, respectively. Energy dispersive spectroscopy (EDS) revealed that the grain boundary precipitates are TiC_x particles despite the very low carbon content (0.046 wt. %).

Table captions

Table 1 Impurity specifications for Grade 1 CP-Ti and some selected Ti alloys [10,16,33].

Table 2 Impurity levels of the starting powders and as-sintered samples (wt.%).

Table 3 Area fraction of carbides and tensile properties of as-HIPed CP-Ti and Ti-Nb alloys [11].

Table 1 Impurity specifications for Grade 1 CP-Ti and some selected Ti alloys [10, 16, 33].

Composition	**N max.**	**C max.**	**H max.**	**Fe max.**	**O max.**	**Standard**
Grade 1 (CP-Ti)	0.03	0.08	0.015	0.20	0.18	ASTM F67
Grade 5 (Ti-6Al-4V)	0.05	0.08	0.015	0.40	0.20	ASTM B348
Ti-10V-2Fe-3Al	0.05	0.05	0.015	2.5	0.16	ASTM 4984
Ti-15V-3Cr-3Al-3Sn	0.05	0.05	0.015	0.25	0.13	ASTM B348
Ti-11.5Mo-6Zr-4.5Sn	0.03	0.10	0.020	0.35	0.18	[16]
Ti-5Al-5V-5Mo-3Cr	0.05	0.10	0.015	0.50	0.18	[16]
Ti-13V-11Cr-3Al	0.05	0.05	0.025	0.35	0.17	[16]
Ti-8Mo-8V-2Fe-3Al	0.05	0.05	0.015	2.4	0.16	[16]
Ti-13Nb-13Zr	0.05	0.08	0.009	0.25	0.15	ASTM F1713-43
Ti-15Mo	0.05	0.10	0.015	0.10	0.20	ASTM F2066-2008

Table 2 - Impurity levels of the starting powders and as-sintered samples (wt.%).

Material	**C**	**O**	**N**
Ti powder	0.00469	0.0744	0.0375
Nb powder	0.0152	0.221	0.0890
CP-Ti	0.0503	0.175	0.0628
Ti-10Nb	0.0562	0.203	0.0678
Ti-16Nb	0.0600	0.255	0.0525
Ti-22Nb	0.0589	0.225	0.0547

Table 3 - Area fraction of carbides and tensile properties of as-HIPed CP-Ti and Ti-Nb alloys [11].

Composition	**Carbide area fraction [%]**	**Ultimate Tensile Strength [MPa]**	**Elongation [%]**	**Young's Modulus [GPa]**
CP-Ti	0	586 ± 1.0	24.2 ± 2.2	116 ± 2.3
Ti-10Nb	0.51 ± 0.08	708 ± 4.5	9.63 ± 1.1	90.1 ± 6.1
Ti-16Nb	0.96 ± 0.15	739 ± 27	4.96 ±0.31	82.2 ± 5.0
Ti-22Nb	1.87 ± 0.61	838 ± 14	1.30 ± 0.41	75.6 ± 7.6

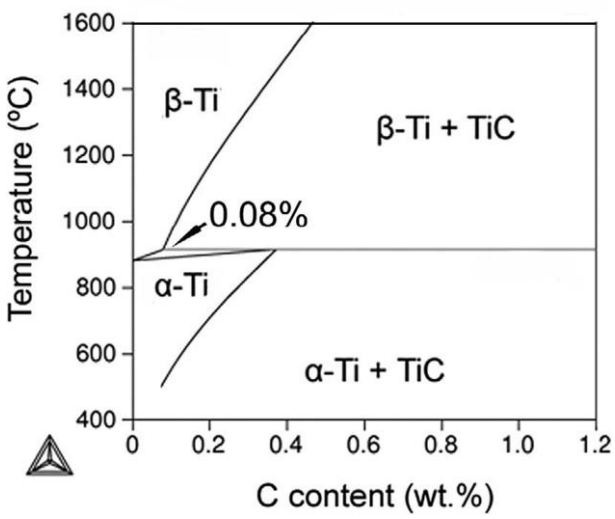

Fig. 1. Ti-C phase diagram up to 1.2 wt.% of carbon, predicted using Thermo-Calc Software 2008 and Ti alloys database V3 (TTTI3) (Courtesy of Yan et al. [10]).

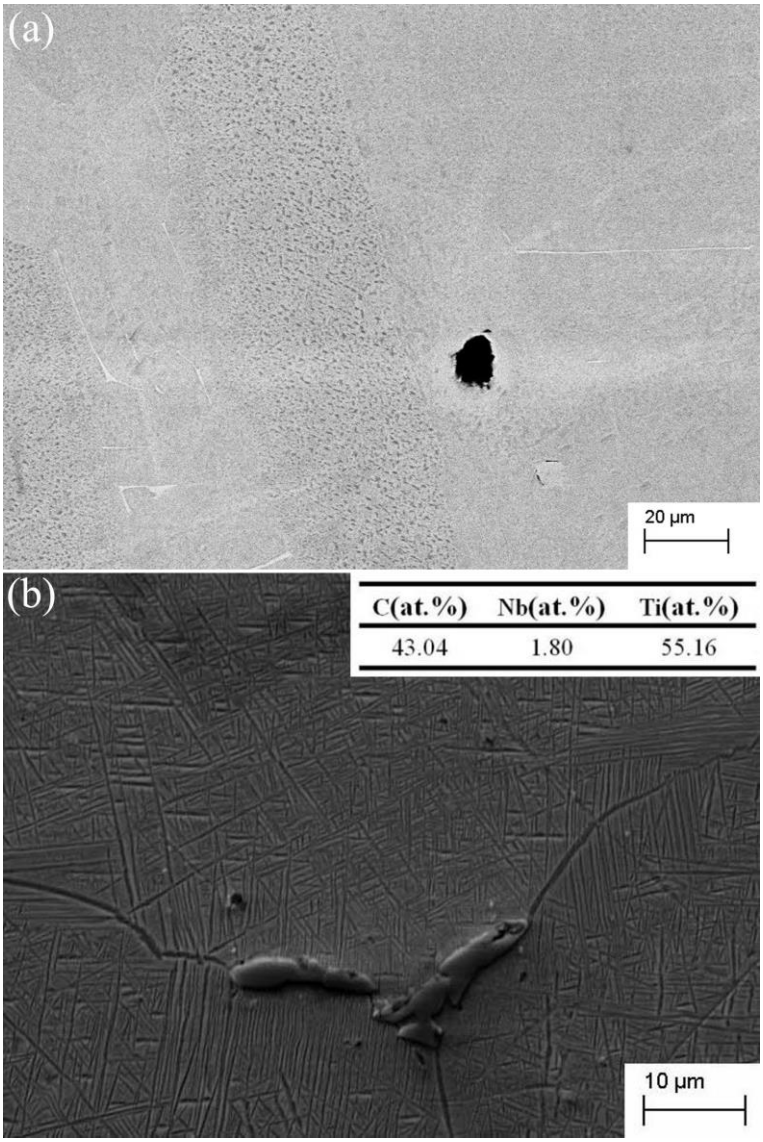

Fig. 2. Microstructures of MIM-processed and sintered (a) CP-Ti and (b) Ti-22Nb samples (scanning electron microscopy (SEM) images). The inset in Fig. 2b shows the EDS results of carbide particles.

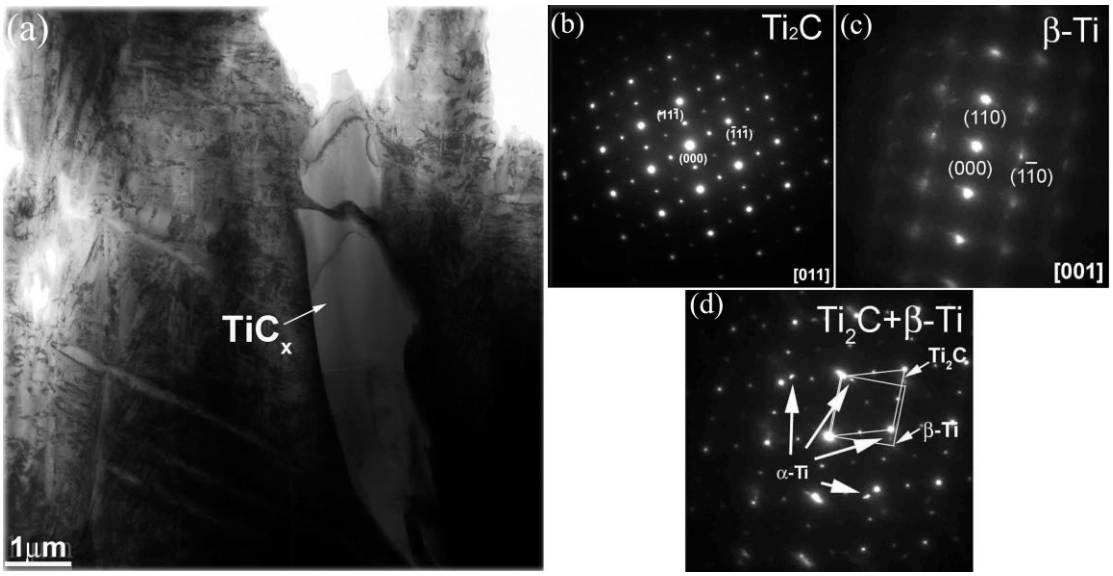

Fig. 3. TEM micrograph and SAED patterns of the as-sintered Ti-22Nb alloy (a) the bright field image, (b) a SAED pattern showing Ti2C reflections from [011]; (c) a SAED pattern showing reflections of the matrix around the Ti2C precipitate, the pattern was found to be β-Ti reflections from [001] and (d) a SAED pattern showing both Ti2C and β-Ti reflections as well as several diffraction spots from α-Ti (Courtesy of Zhao et al. [11]).

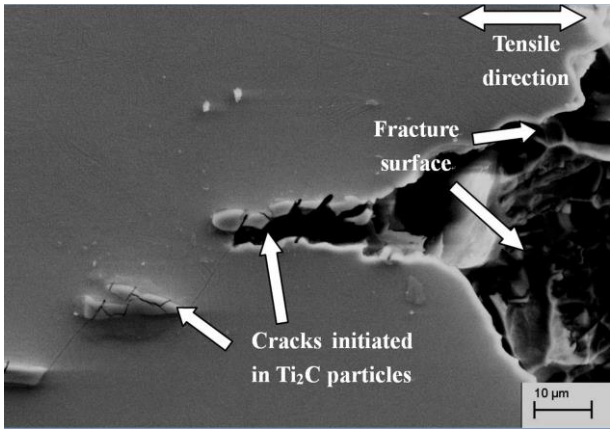

Fig. 4. SEM micrograph along the longitudinal section of a fractured as-HIPed Ti-22Nb sample showing fragmented carbide particles and microcracks.

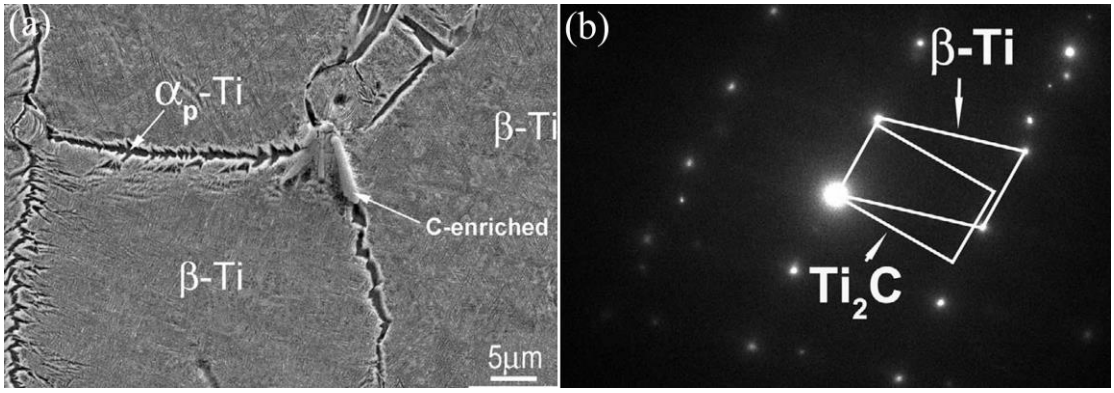

Fig. 5. (a) SEM image of the as-sintered Ti-15Mo alloy and (b) an overlap of the SAED patterns of the TiCx particles and the adjacent β-Ti matrix (Courtesy of Yan et al. [10]).

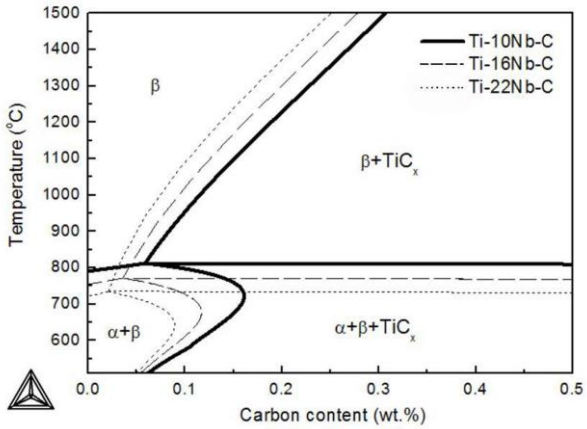

Fig. 6. Pseudo-binary phase diagrams of (Ti-10Nb)-C, (Ti-16Nb)-C and (Ti-22Nb)-C up to 0.5 wt.% of carbon predicted using Thermo-Calc software (Courtesy of Zhao et al. [32]).

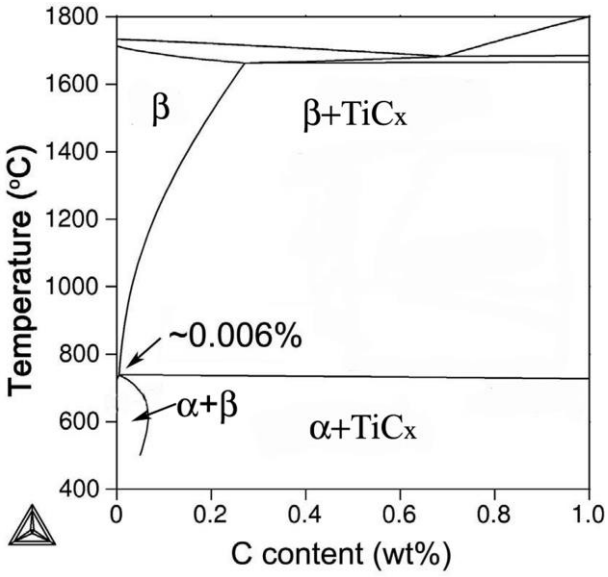

Fig. 7. Pseudo binary (Ti-15Mo)-C phase diagram up to 1.0 wt.% of C predicted using Thermo-Calc software (Courtesy of Yan et al. [10]).

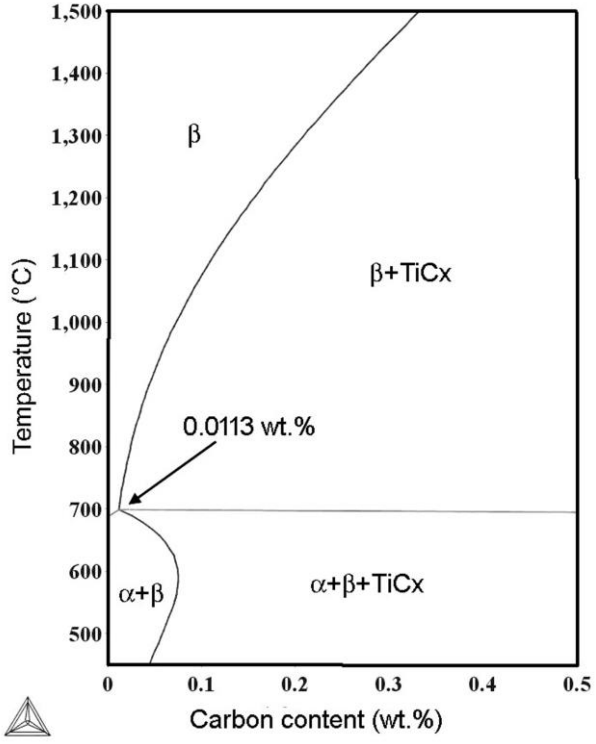

Fig. 8. Pseudo binary (Ti-15V)-C phase diagram up to 0.5 wt.% of carbon predicted using Thermo-Calc software.

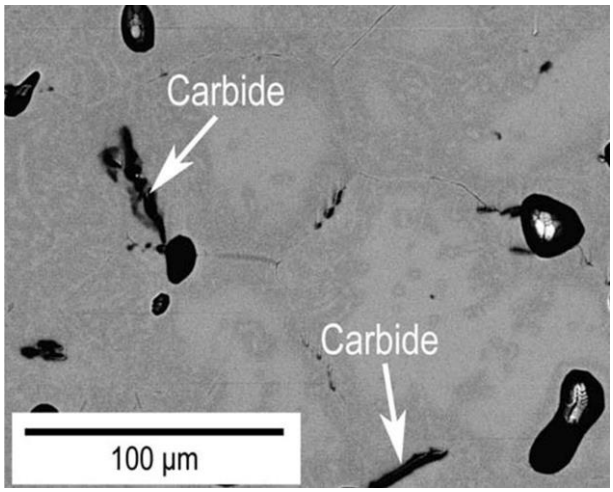

Fig. 9. Microstructure of aged MIM-processed Ti-15V-3Al-3Sn-3Cr (Ti-15333) alloy. Samples were sintered at 1400 ℃ for 2 h after MIM and then aged at 500 ℃ for 12 h. The C, O and N contents were about 0.046 wt.%, 0.21 wt.% and 0.024 wt.%, respectively. Energy dispersive spectroscopy (EDS) revealed that the grain boundary precipitates are TiCx particles despite the very low carbon content (0.046 wt. %).